

# Synthesis of WO<sub>3</sub> Nanorods and Their Excellent Ethanol Gas-Sensing Performance

Jingkun Xiao<sup>a</sup>, Yanhan Che<sup>a</sup>, Bowen Lv<sup>a</sup>, Massamba-Courtoisjoanes Benedicte<sup>a</sup>, Guoqing Feng<sup>a</sup>,  
Tianjun Sun<sup>b\*</sup>, Chengwen Song<sup>a</sup> 

<sup>a</sup>Dalian Maritime University, College of Environmental Science and Engineering, 1 Linghai Road,  
Dalian 116026, China

<sup>b</sup>Dalian Maritime University, Marine Engineering College, Dalian 116026, China

Received: September 22, 2020; Revised: January 5, 2021; Accepted: February 21, 2021

WO<sub>3</sub> nanorods were synthesized via a simple hydrothermal approach. Their microstructure and morphology were analyzed with x-ray diffraction, scanning electron microscope and x-ray photoelectron spectroscopy. The effects of reaction temperature, reaction time, and citric acid concentration, on the gas-sensing performance of WO<sub>3</sub> nanorods were investigated. The optimized response value of WO<sub>3</sub> sensor to ethanol gas (100 ppm) was 26.48, with a response time of 1 s under a low operating temperature (160 °C). The recovery capability and stability of the gas sensor were tested and discussed. Additionally, the working principle of WO<sub>3</sub> sensor was proposed. In comparison to the sensors published by previous researchers, the WO<sub>3</sub> sensor has shown great potential.

**Keywords:** WO<sub>3</sub>, gas sensor, response, nanorods, ethanol.

## 1. Introduction

Along with the development of human society, air pollution has become a serious environmental problem. Ethanol gas is a representative of volatile organic compounds (VOCs), and its prevention and control standards have been continuously improved in recent years<sup>1</sup>. Large and continuous expose to ethanol gas can cause serious health problems (to human beings), like dyspnea, internal organ damage, etc<sup>2</sup>. In order to prevent economic loss and environmental pollution, there is an imminent need for highly sensitive and practical gas sensor.

In recent years, some types of gas sensors have been developed. Among them, the most attractive type of gas sensors is the metal oxide semiconductor (MOS). ZnO<sup>3</sup>, CoO<sup>4</sup>, NiO<sup>5</sup>, and other metal oxides have shown great performance in gas-sensing applications. WO<sub>3</sub> is a metal oxide of n-type semiconductor, with superior performance in various fields. At present, WO<sub>3</sub> has been widely used in catalysts<sup>6</sup>, solar cells<sup>7</sup>, gas sensors<sup>8</sup>, etc. In gas sensors, WO<sub>3</sub> also shows high performance, fast response, and outstanding stability. Up to now, WO<sub>3</sub> has been widely investigated, owing to its easy structure control and numerous synthetic methods. For gas-sensitive materials, structural difference will affect the gas-sensing performance, and the structure of the material is closely related to the synthesis method.

Nowadays, the methods used to synthesize WO<sub>3</sub> have been widely developed, such as sol-gel, template, thermal decomposition, etc. Additionally, the developed WO<sub>3</sub> structures are nanotubes<sup>9-11</sup>, nano films<sup>12</sup>, nano tablets<sup>13</sup>, nano microspheres<sup>14</sup>, etc. Among them, one-dimensional materials were widely explored on account of their simple structure and easy preparation. Cai et al. directly grew single crystal WO<sub>3</sub> nanowires on FTO substrate by hydrothermal

method. The response of nanowires towards 500 ppm NO at 300 °C was 37<sup>15</sup>. Leng et al. synthesized WO<sub>3</sub> nanofibers by electrospinning. The response of WO<sub>3</sub> nanofibers to 100 ppm NH<sub>3</sub> reached 5.5<sup>16</sup>. An et al.<sup>17</sup> used TeO<sub>2</sub> nanowire templates to fabricate WO<sub>3</sub> nanotubes, which showed a response of 676.57 to 5 ppm NO<sub>2</sub> at 300 °C. These works have proved that WO<sub>3</sub> was an excellent gas-sensitive material, but several essential issues still required to be solved. For instance, the response time of the gas sensor to the target gas was long, and the working principle of the gas sensor was still unclear. As a representative of one-dimensional materials, compared with other one-dimensional structures, nanorods have a rough surface, more surface-active vacancies, which can speed up the adsorption and diffusion of gas molecules on the surface of the material, thereby reducing the response time. Considering the unique porous morphology of WO<sub>3</sub> nanorods, changing the synthesis conditions of the reaction and further ameliorating the morphology of the material can improve the gas sensitivity of the WO<sub>3</sub> sensor.

In this work, WO<sub>3</sub> nanorods were synthesized by hydrothermal method. Meanwhile, their microstructure and composition were analyzed. The gas-sensitive performance of WO<sub>3</sub> was investigated by controlling reaction temperature, reaction time and citric acid concentration. Furthermore, the selectivity and the response recovery ability of WO<sub>3</sub> were systematically investigated, and the sensing mechanism of WO<sub>3</sub> was analyzed.

## 2. Experimental

### 2.1. Chemicals and materials

Ammonium tungstate (NH<sub>4</sub>)<sub>10</sub>(H<sub>2</sub>W<sub>12</sub>O<sub>42</sub>) · 16H<sub>2</sub>O, citric acid (C<sub>6</sub>H<sub>8</sub>O<sub>7</sub> · H<sub>2</sub>O) and anhydrous ethanol (CH<sub>3</sub>CH<sub>2</sub>OH) were

\*e-mail: [suntianjun@dlnu.edu.cn](mailto:suntianjun@dlnu.edu.cn)

supplied by Sinopharm Chemical Reagent Co., Ltd. (China). The water used in the experiment was deionized water.

## 2.2. Preparation of $WO_3$ nanorods

2.0 g of  $(NH_4)_{10}(H_2W_{12}O_{42}) \cdot 16H_2O$  and 0.5 g of  $C_6H_8O_7 \cdot H_2O$  were added to 80 ml deionized water under stirring. Furthermore, the solution was stirred for more than 30 min at 25 °C until the drug was completely dissolved. The mixture was sealed into Teflon-lined autoclave of 100 ml and heated at 160 °C for 24 h. Afterwards, the Teflon-lined autoclave was placed in a dry and ventilated place, to allow the solution to be cooled naturally. The solid matter was collected by suction filtration. The collected solid matter was consecutively washed three times with deionized water and with absolute ethanol. Ultimately, the collected  $WO_3$  solid matter was dried at 60 °C for 10 h. The  $WO_3$  nanorods synthesis process is shown in Figure 1.

In order to investigate the influence of synthesis conditions on the nanostructures of  $WO_3$ , the synthesis conditions were changed by controlling three variables: the reaction temperature, the reaction time and the citric acid concentration. The summary of synthesis conditions of  $WO_3$  was shown in Table 1.

**Table 1.** Summary of synthesis conditions of  $WO_3$ .

Sample	Reaction temperature	Reaction time	Citric acid concentration
$WO_3$ -1	120 °C	24 h	0.03 mol/L
$WO_3$ -2	160 °C	24 h	0.03 mol/L
$WO_3$ -3	200 °C	24 h	0.03 mol/L
$WO_3$ -4	160 °C	12 h	0.03 mol/L
$WO_3$ -5	160 °C	36 h	0.03 mol/L
$WO_3$ -6	160 °C	48 h	0.03 mol/L
$WO_3$ -7	160 °C	36 h	0.02 mol/L
$WO_3$ -8	160 °C	36 h	0.04 mol/L
$WO_3$ -9	160 °C	36 h	0.05 mol/L

## 2.3. Characterization

The crystallization behavior of these samples was analyzed by X-ray diffraction (XRD, D/max-2400) with Cu-K $\alpha$  radiation at the scanning range of  $2\theta$  from 10° to 80°. The morphologies of  $WO_3$  nanomaterials were investigated by the scanning electron microscope (SEM) (Philips XL30 FEG). The X-ray photoelectron spectroscopy (XPS) of the  $WO_3$  nanomaterials was analyzed by Thermo SCIENTIFIC ESCALAB 250 spectrometer using an Al-K $\alpha$  source.

The lattice parameters, average grain size and unit cell volume of different  $WO_3$  nanostructures were investigated. The formula is as follows, where  $\lambda$  is the X-ray wavelength - 0.1546 nm,  $\theta$  is the diffraction peak angle,  $\beta$  is the half height width of the diffraction peak.

$$D_{hkl} = \frac{0.89\lambda}{\beta \cos \theta} \quad (1)$$

## 2.4. Fabrication and measurement of the gas sensor

A small amount of  $WO_3$  nanomaterials was grounded in an agate mortar. The  $WO_3$  nanomaterials powder was mixed thoroughly with ethanol, and the mixture was spread onto the external surface of  $Al_2O_3$  tube, composed of gold electrode and four Pt wires. A Ni-Cr heating wire was inserted into the  $Al_2O_3$  tube to constitute a small gas-sensing device. To complete the gas sensor, the four Pt wires and the Ni-Cr heating wire were welded on the metal pedestal with a welding machine. Afterwards, the gas sensor was inserted into the aging plate and then aged under a low heating voltage. The aging time exceeded 24 h. The gas sensing performance was measured by the intelligent gas sensing and measuring system of WS-30A (Zhengzhou Weisheng Electronic Technology Co., Ltd., China). The schematic diagram is shown in Figure 2. The sensing response of the gas sensor (s) was defined as the relative change of resistance.  $R_a$  and  $R_g$  are the resistances measured by  $WO_3$  sensor in

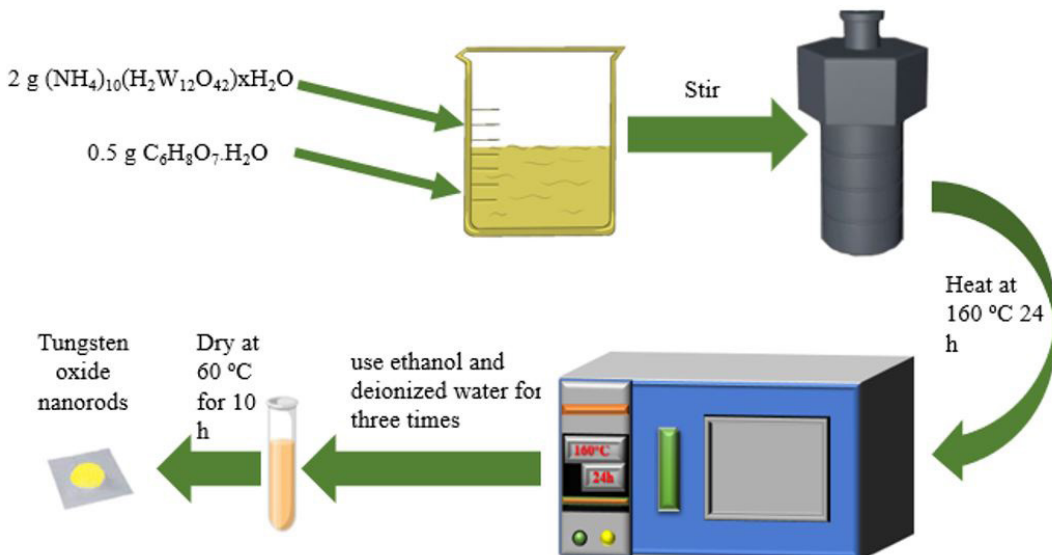


**Figure 1.** Schematic illustration of the synthesis process of  $WO_3$ .

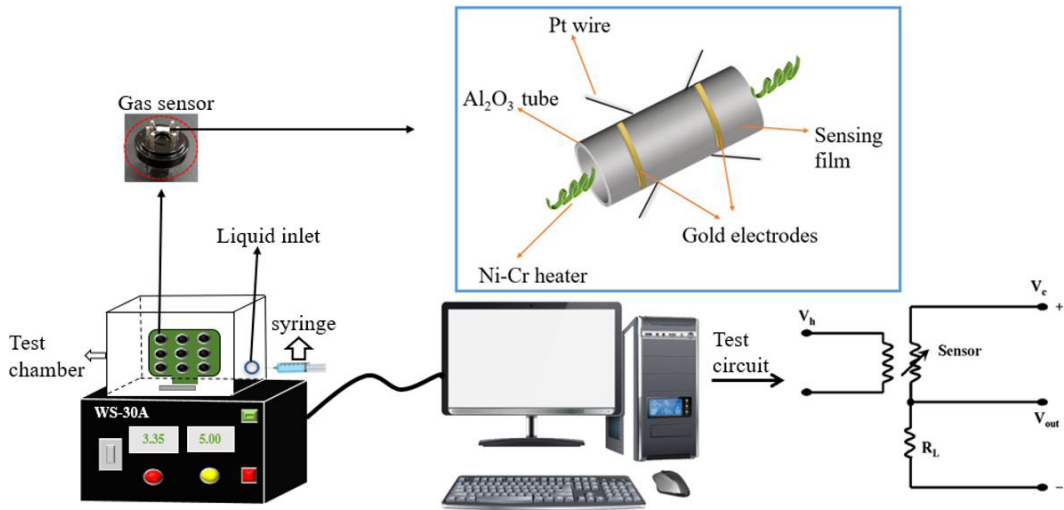


**Figure 2.** Schematic diagram of the WS-30A gas-sensing measurement system.

air and target gas, respectively.  $R_L$  is the load resistance. The formulas used to calculate the different resistances and the sensing response are presented as follows, where  $V_c$  is the circuit voltage (5 V),  $V_a$  and  $V_g$  are the voltages measured by WO<sub>3</sub> sensor in air and target gas. The sensor resistance can be calculated by changing the output voltage ( $V_{OUT}$ ):

$$R_a = \frac{(V_c / V_a - 1)}{R_L} \quad (2)$$

$$R_g = \frac{(V_c / V_g - 1)}{R_L} \quad (3)$$

$$S = \frac{R_a}{R_g} \quad (4)$$

### 3. Results and Discussion

#### 3.1. Morphology and structure of WO<sub>3</sub>

Figure 3 shows the representative XRD of the WO<sub>3</sub> nanomaterials synthesized at 160 °C, with reaction time 36 h and 0.03 mol/L citric acid. All the samples show the WO<sub>3</sub> phase. As observed, the characteristic diffraction peaks at  $2\theta$  are 14.0°, 26.8°, 28.2°, 33.6°, 36.6°, 50.0°, 55.3° and 63.5°, which are assigned to (100), (001), (200), (111), (201), (220), (202) and (401) crystal faces, and are basically consistent with PDF card (JCPDS No. 33-1387). In addition, no other diffraction peaks are found, thus the samples are all hexagonal phase crystals WO<sub>3</sub>. The lattice parameters, unit cell volume and average grain size of WO<sub>3</sub> are shown in Table 2.

Figure 4 depicts the SEM micrographs of WO<sub>3</sub> at 160 °C, 36 h and 0.03 mol/L citric acid. The results demonstrate that the synthesized WO<sub>3</sub> nanomaterials are short rods. The low-magnification SEM is performed to show the existence of WO<sub>3</sub> nanorods. Apparently, it can be observed that the

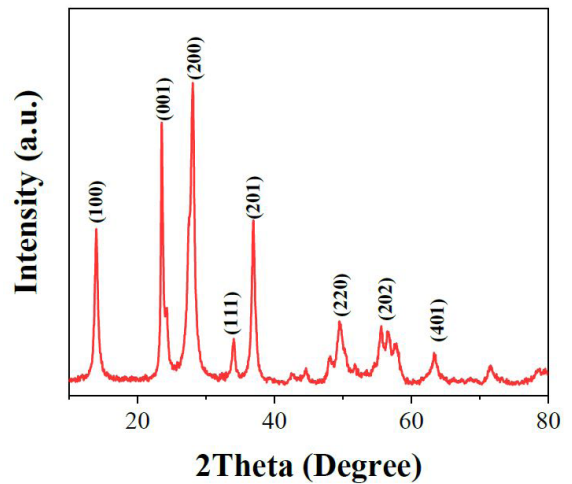


**Figure 3.** XRD patterns of WO<sub>3</sub> samples.

**Table 2.** Lattice parameters, unit cell volume and average grain size of WO<sub>3</sub>.

Sample	Lattice parameters (Å)			Unit cell volume (Å <sup>3</sup> )	Average crystallite size (nm)
	a	b	c		
WO <sub>3</sub>	6.3249	4.4969	3.7720	107.28	33.2

nanorods are obtained and with rough surfaces. The shape of nanorods can be clearly observed by the magnified SEM of Figure 4a and Figure 4c. We can see that nanorods formed complete and distributed uniformly on a large scale. These results correspond to the average grain size calculated in XRD.

X-ray photoelectron spectroscopy (XPS) clarify the chemical binding state of the sample. X-ray photoelectron spectroscopy is shown in Figure 5. The results presented in Figure 5 show that the sample is composed of three elements: C, W and O. Among these elements, the element C is the impurity introduced by the target gas. Because of the asymmetry of the peak at a low

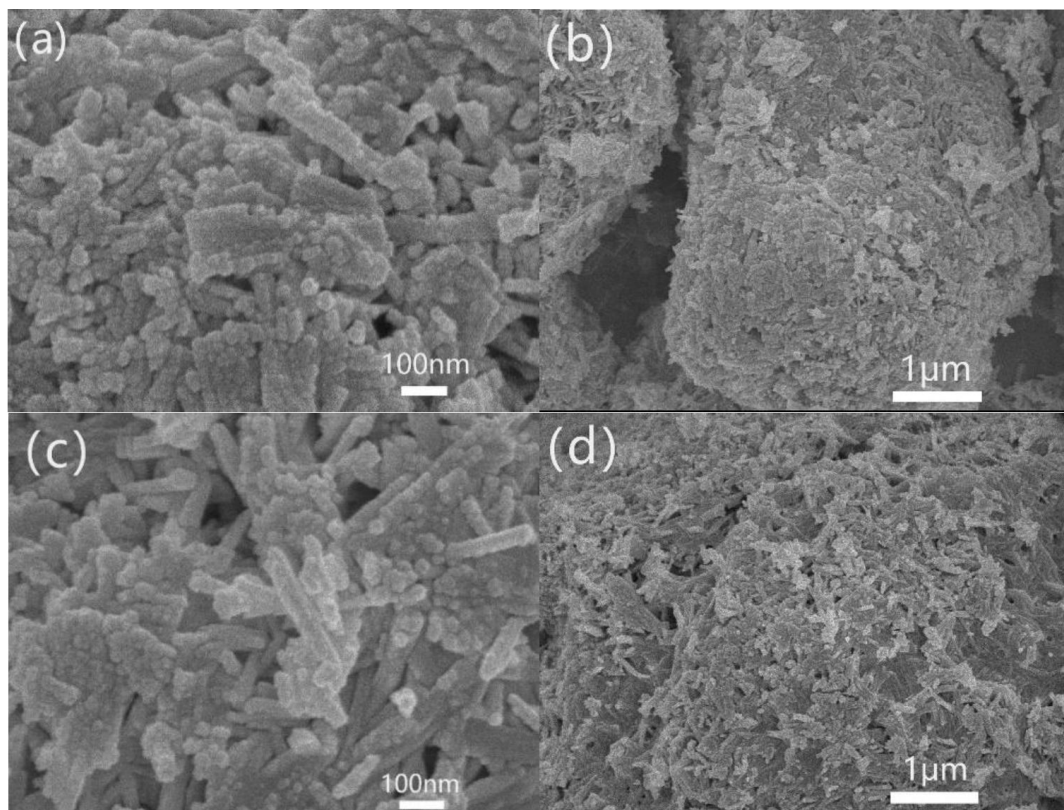


**Figure 4.** SEM images of  $\text{WO}_3$  synthesized at 160 °C, 36 h and 0.03 mol/L citric acid.

binding energy, another bimodal is used to clearly present the W4f peak. It means that tungsten trioxide is deficient in oxygen, which supports the electronic transport properties of the material by the introduction of donor electrons<sup>18-23</sup>. The spectrum of O(1s) shows an asymmetrical line. The main peak in the binding energy is about 531.1 eV. This is due to the single bond existing between tungsten and oxygen<sup>18</sup>. In Figure 5b, the high binding energy peaks at 36.08 eV and 38.12 eV correspond to  $\text{W4f}_{7/2}$  and  $\text{W4f}_{5/2}$  respectively. The peak value of  $\text{W4f}_{7/2}$  at 36.08 eV is higher than that of  $\text{W4f}_{5/2}$  at 38.12 eV, and the peak area ratio is about 4:3, which confirms that the element exists as  $\text{WO}_3$ <sup>24,25</sup>. Based on the analysis results, the molecular formula of the sample can be determined as  $\text{WO}_3$ .

### 3.2. Gas sensing properties of $\text{WO}_3$ nanomaterials

The performance of gas sensors with metal oxide nanomaterials depends largely on the operating temperature. Consequently, the sensing performance of  $\text{WO}_3$  exposed to 100 ppm ethanol was investigated at a given operating temperature range (100-260 °C). Figure 6a reveals the response of the gas sensor to the reaction temperature, taken as a variable. At first, the sensitivity of the three materials ( $\text{WO}_3$ -1,  $\text{WO}_3$ -2,  $\text{WO}_3$ -3) increased. Afterwards, their sensitivity decreased. Among the three materials,  $\text{WO}_3$ -1 reached the maximum response when the operating temperature was 200 °C. However,  $\text{WO}_3$ -1 and  $\text{WO}_3$ -3 did not show excellent gas-sensing performance. The results imply that  $\text{WO}_3$ -1 failed to form a complete nanorod

during the preparation process, which resulted in the material being unable to deoxidize. On the contrary,  $\text{WO}_3$ -3 has shown a bad performance. This may be because the high synthesis temperature destroys the formed  $\text{WO}_3$  crystal nucleus<sup>26</sup>, which weakens its ability to combine with adsorbed oxygen. As a result, comparing the images and data, the optimal reaction temperature was determined as 160 °C. Figure 6b illustrates the comparative sensing response of the gas sensors at different reaction time. The sensitivity of the three samples of gas sensors first increased, then decreased rapidly. The sample  $\text{WO}_3$ -5 shows the highest response with 26.48. The responses of  $\text{WO}_3$ -4 and  $\text{WO}_3$ -2 both exceeded 8, but  $\text{WO}_3$ -6 showed almost no response. The reason behind those results may be that  $\text{WO}_3$  gradually formed nanorod-like structures with the increase in reaction time, and the rod-like structures were most likely completely formed at 36 h. However, at 48 h, the original structures were broken and recombined into a mass, which reduced the active vacancies on the surface of the material. Figure 6c shows the response of the material to the citric acid concentration, taken as a variable. From the figure the optimum citric acid concentration is 0.03 mol/L, and the optimum operating temperature is 160 °C. Figure 7 reveals the response of  $\text{WO}_3$  nanorods towards different ethanol gas concentrations. The responses are 1.08, 6.8, 18.2, 22.2, and 26.52, respectively. It can be observed from the figure that when the concentration of ethanol gas is lower than 100 ppm, the response value of the gas sensors increases rapidly. As the concentration continues to increase to 300 ppm, the response of the gas sensors increases gently. These trends are caused by

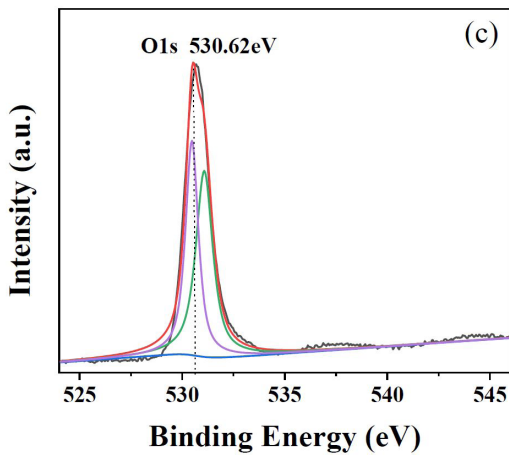
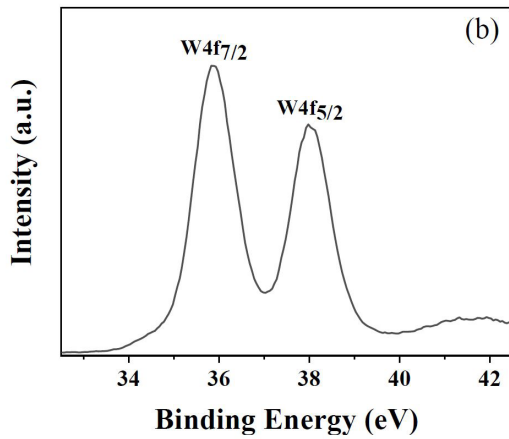
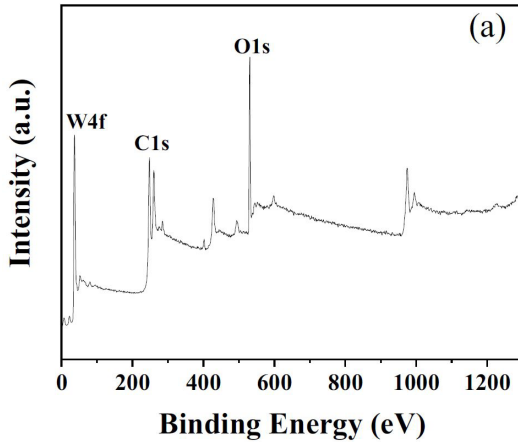


**Figure 5.** XPS spectrum of WO<sub>3</sub>, (a) wide scan spectrum, (b) W4f spectrum, and (c) O1s spectrum.

the saturation of gas molecules and surface-active vacancy, and the stable equilibrium of adsorption rate and desorption rate.

Under the optimum operating temperature of 160 °C, the response and recovery times of WO<sub>3</sub>-5 were investigated. The response and recovery curve according to the time is

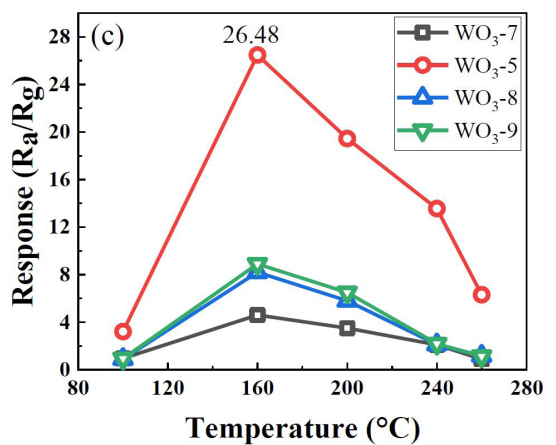
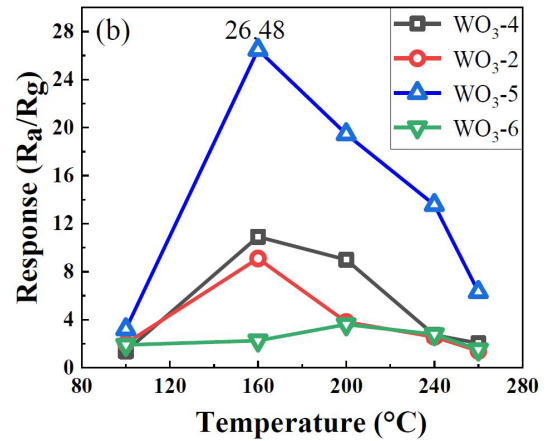
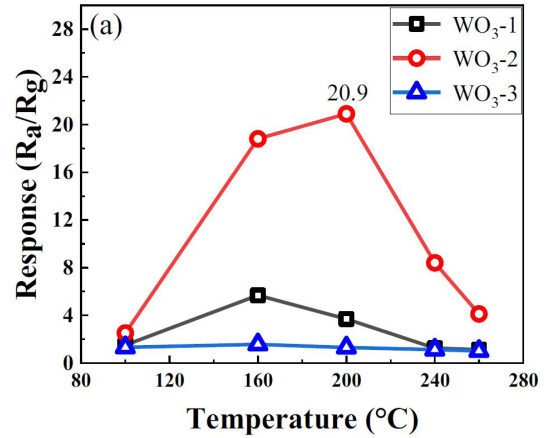


**Figure 6.** Responses of the WO<sub>3</sub> sensors to ethanol (100 ppm) under different reaction conditions: (a) reaction temperatures, (b) reaction time, and (c) concentrations of the citric acid addition.

shown in Figure 8, corresponding to 20, 50, 100, 200 and 300 ppm ethanol gas, respectively. When the ethanol gas was injected, the sensor response increased rapidly, with a response time of about 1 s. After the sensor was placed in contact with the air, the sensor response decreased gradually,

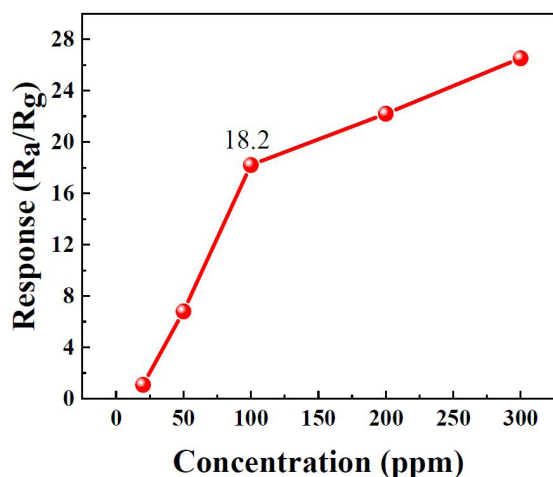


Figure 7. Sensitivity plot of  $WO_3$  gas sensor under different ethanol concentration.

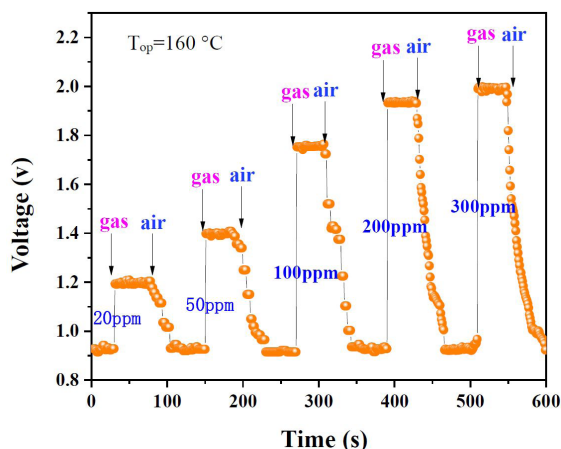


Figure 8. Response and recovery curve of  $WO_3$ -5 gas sensor at optimum operating temperature ( $160\text{ }^\circ\text{C}$ ).

with a recovery time of about 30 s. The response of the device nearly returned to its initial state after detecting the ethanol gas and being in contact with the air, which indicates that the  $WO_3$  sensor has a superior repeatability.

The selectivity of  $WO_3$  nanorods to ethanol, benzene, dichloromethane, formaldehyde, and n-butanol at a concentration of 100 ppm was respectively investigated. The results are shown in Figure 9. The sample  $WO_3$ -5 shows an excellent response to ethanol, followed by benzene and acetone. These results show that the sample  $WO_3$ -5 has an excellent selectivity towards reducing gas in a gas environment.

Table 3 mainly introduces the response of  $WO_3$  with different morphologies to 100 ppm ethanol gas. According to the published data, the  $WO_3$  nanorods prepared in this work demonstrate high sensitivity than most of nanomaterials<sup>27-29</sup>, and they still possess great advantages compared to  $WO_3$  nanofilms<sup>30</sup>. Although the response of the  $WO_3$  nanorods prepared in this work is lower than the urchin-like  $WO_3$ <sup>1</sup> and Spider web  $WO_3$ <sup>31</sup>, the response and recovery times of these two materials are low.  $WO_3$  nanorods can respond to the target gas rapidly and have a fast recovery time, which

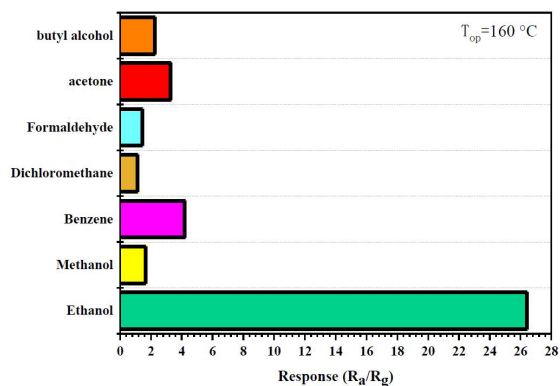


Figure 9. Sensitivity histogram of  $WO_3$ -5 gas sensor under different gases.

is very important for sensor applications. Compared to all the examples given,  $WO_3$  nanorods did not only show a high response, but also worked at a low optimal operating temperature, which is suitable for low temperature operations.

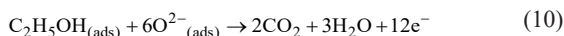
### 3.3. Gas sensing mechanism of $WO_3$ sensors

In most cases, when the metal oxide gas sensing materials are in contact with dry air, only physical adsorption occurs on their surface. However, when they are placed in contact with reducing gases such as ethanol vapor, both physical adsorption and chemical adsorption occur. The principle of chemical adsorption is presented as follows:

At first, the gas-sensitive material physically adsorbs the oxygen present in the air. After the oxygen in the air is adsorbed on the surface of the gas-sensitive material, chemical adsorption occurs, and electrons obtained from the gas-sensitive material form the oxygen anions ( $O_2^{-2}$ ,  $O_2^-$ ,  $O^{2-}$ ), as shown by the following equations:



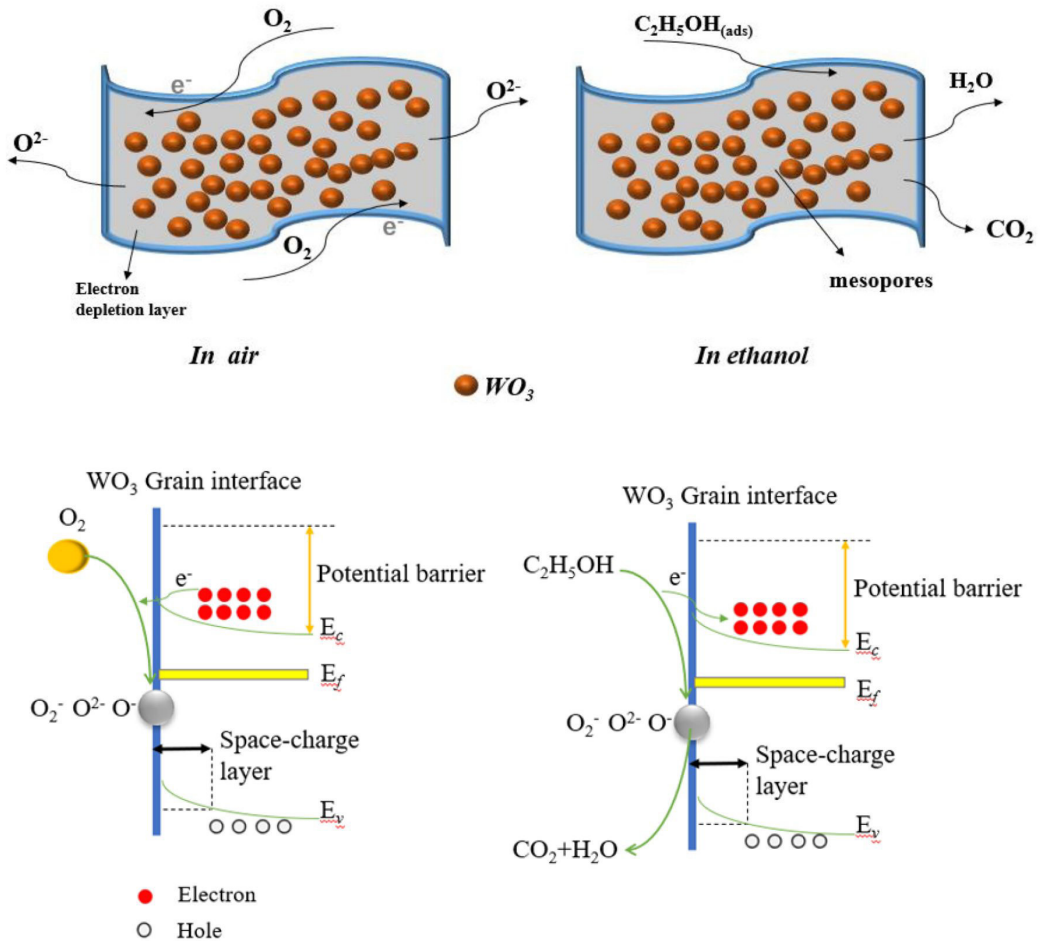
At that moment, the conductivity of  $WO_3$  is weak. When the gas sensing materials are placed in contact with the reducing gas, the physical adsorption and the chemical adsorption occur at the same time, which is accompanied by the ionization of the reducing gas, as presented in the following equations:



When the concentration of the gas continues to increase, the chemical ionization of the reducing gas on the surface of the material also increases. This phenomenon provides more conductive particles to the sensing material, which in turn

**Table 3.** Gas sensors for ethanol detection reported in literatures and in this work.

Sensing materials	Concentration (ppm)	Operating temperature (°C)	Response (S)	Response time (s)	Recovery time (s)	References
WO <sub>3</sub> nanorod	100	160	26.48	1	30	In this work
WO <sub>3</sub> nanospheres	100	250	16.2	34.2	35.6	27
WO <sub>3</sub> nanoscale	100	-	15.6	10-15	30-35	28
Urchin-like WO <sub>3</sub>	100	350	68.56	28	12	1
WO <sub>3</sub> nanorod	100	275	6-7	141	148	29
WO <sub>3</sub> deposition film	100	250	15.2	-	-	30
Spider web WO <sub>3</sub>	100	300	72	-	-	31

**Figure 10.** Schematic diagram of WO<sub>3</sub> sensor sensing mechanism.

improves the conductivity of the material, then ultimately reflects on the change in the response of material towards the reducing gas.

A graphical diagram of the ethanol-sensing mechanism on the surface of the WO<sub>3</sub> sensor is shown in Figure 10. WO<sub>3</sub> is an n-type semiconductor material. When the ethanol gas (C<sub>2</sub>H<sub>5</sub>OH) passes into the test environment, the anions O<sup>2-</sup> adsorbed on the surface of WO<sub>3</sub> react with the C<sub>2</sub>H<sub>5</sub>OH. During the reaction, C<sub>2</sub>H<sub>5</sub>OH loses electrons, and the electrons obtained from the oxygen atoms return to WO<sub>3</sub>. The electron transfer during the adsorption process increases the carrier concentration in WO<sub>3</sub>, leading to an

increase in conductivity of the sensor and a reduction of the load voltage of the sensor. Therefore, by changing the type and concentration of the adsorbed gas, the load voltage of the sensor can be adjusted.

#### 4. Conclusions

We reported our work on the preparation of WO<sub>3</sub> nanorods using the hydrothermal method. According to the response of the material to ethanol gas under different synthesis conditions, the influence of the reaction conditions on the gas sensing performance of the sensors was analyzed.

The plausible formation mechanism of WO<sub>3</sub> nanorods was discussed in the light of the SEM figures of WO<sub>3</sub> synthesized by different reaction temperatures, reaction time and citric acid concentrations. The results showed that the morphology of WO<sub>3</sub> has a significant impact on the sensitivity of the gas sensor. The gas sensitivity of materials under different synthesis conditions were tested. In the presence of 100 ppm ethanol, the response of the WO<sub>3</sub>-5 (reaction temperature 160 °C, reaction time 36 h and citric acid concentration 0.03 mol/L) sensor was 26.48. WO<sub>3</sub> could recognize many reducing gases, which showed its excellent selectivity. WO<sub>3</sub> had a favorable recovery ability, which allowed the material to quickly identify the target gas in a transitory time and to quickly return to the original state of its response. In addition, the sensing mechanism of WO<sub>3</sub> sensor for ethanol was explained. Compared with the previous literatures, WO<sub>3</sub> showed a great potential in the rapid detection of ethanol.

## 5. Acknowledgements

This work was supported by Program for Liaoning Innovative Talents in University, and Key Research & Development Project of Liaoning Province (2017308005).

## 6. References

- Zhang D, Cao Y, Wu J, Zhang X. Tungsten trioxide nanoparticles decorated tungsten disulfide nanoheterojunction for highly sensitive ethanol gas sensing application. *Appl Surf Sci.* 2020;503:144063.
- Mirzaei A, Park S, Sun G, Kheel H, Lee C, Lee S. Fe<sub>2</sub>O<sub>3</sub>/Co<sub>3</sub>O<sub>4</sub> composite nanoparticle ethanol sensor. *J Korean Phys Soc.* 2016;69(3):373-80.
- Thepnurat M, Chairuangri T, Hongsith N, Ruankham P, Choopun S. Realization of Interlinked ZnO tetrapod networks for UV sensor and room-temperature gas sensor. *ACS Appl Mater Interfaces.* 2015;7(43):24177-84.
- Zhang D, Jiang C, Li P, Sun Y. Layer-by-layer self-assembly of Co<sub>3</sub>O<sub>4</sub> nanorod-decorated MoS<sub>2</sub> nanosheet-based nanocomposite toward high-performance ammonia detection. *ACS Appl Mater Interfaces.* 2017;9(7):6462-71.
- Nakate U, Ahmad R, Patil P, Yu Y, Hahn Y. Ultra thin NiO nanosheets for high performance hydrogen gas sensor device. *Appl Surf Sci.* 2020;506:144971.
- Liu X, Zhai H, Wang P, Zhang Q, Wang Z, Liu Y, et al. Synthesis of a WO<sub>3</sub> photocatalyst with high photocatalytic activity and stability using synergetic internal Fe<sup>3+</sup> doping and superficial Pt loading for ethylene degradation under visible-light irradiation. *Catal Sci Technol.* 2019;9:652-8.
- Zou L, Zhong Q, Liu Q. Preparation and characterization of microporous nano-tungsten trioxide and its photocatalytic activity after doping rare earth. *J Rare Earths.* 2006;24(1):60-6.
- Jung G, Jeong Y, Hong Y, Wu M, Hong S, Shin W, et al. SO<sub>2</sub> gas sensing characteristics of FET- and resistor-type gas sensors having WO<sub>3</sub> as sensing material. *Solid-State Electron.* 2020;165:107747.
- Chi X, Liu C, Liu L, Li Y, Wang Z, Bo X, et al. Tungsten trioxide nanotubes with high sensitive and selective properties to acetone. *Sens Actuators B Chem.* 2014;194:33-7.
- Koo W, Choi S, Kim N, Jang J, Kim I. Catalyst-decorated hollow WO<sub>3</sub> nanotubes using layer-by-layer self-assembly on polymeric nanofiber templates and their application in exhaled breath sensor. *Sens Actuators B Chem.* 2016;223(223):301-10.
- An S, Park S, Ko H, Lee C. Fabrication of WO<sub>3</sub> nanotube sensors and their gas sensing properties. *Ceram Int.* 2014;40(1):1423-9.
- Hu M, Zeng J, Wang W, Chen H, Qin Y. Porous WO<sub>3</sub> from anodized sputtered tungsten thin films for NO<sub>2</sub> detection. *Applied Surface Science.* 2011;258(3):1062-68.
- Wu C, Zhu Z, Huang S, Wu R. Preparation of palladium-doped mesoporous WO<sub>3</sub> for hydrogen gas sensors. *J Alloys Compd.* 2019;776:965-73.
- Huang J, Xu X, Gu C, Yang M, Yang M, Liu J. Large-scale synthesis of hydrated tungsten oxide 3D architectures by a simple chemical solution route and their gas-sensing properties. *J Mater Chem.* 2011;21:13283-9.
- Cai Z, Li H, Yang X, Guo X. NO sensing by single crystalline WO<sub>3</sub> nanowires. *Sens Actuators B Chem.* 2015;219:346-53.
- Leng J, Xu X, Lv N, Fan H, Zhang T. Synthesis and gas-sensing characteristics of WO<sub>3</sub> nanofibers via electrospinning. *J Colloid Interface Sci.* 2011;356(1):54-7.
- An S, Park S, Ko H, Lee C. Fabrication of WO<sub>3</sub> nanotube sensors and their gas sensing properties. *Ceram Int.* 2014;40(1):1423-9.
- Erohid S, Heidari S, Jafari A, Asgary S. Effect of growth time on structural, morphological and electrical properties of tungsten oxide nanowire. *Appl Phys, A Mater Sci Process.* 2018;124(8):1-9.
- Shahidi S, Jafari A, Sharifi S, Ghoranneviss M. Deposition of nano tungsten oxide on glass mat using hot filament chemical vapor deposition for high catalytic activity. *High-Temp Mater Process.* 2016;35(5):515-21.
- Jafari A, Ghoranneviss M, Meshkani S. The hydrogen plasma effect on the tungsten oxide nano-sheets in Tokamak. *J Fusion Energy.* 2016;35(2):306-11.
- Liu L, Sheng Y, Liu M, Dienwiebel M, Zhang Z, Dastan D. Formation of the third bodies of steel sliding against brass under lubricated conditions. *Tribol Int.* 2019;140:105727.
- Liu M, Li C, Liu L, Ye Y, Dastan D, Garmestani H. Inhibition of stress corrosion cracking in 304 stainless steel through titanium ion implantation. *J Mater Sci Technol.* 2020;36:284-92.
- Ghoranneviss Z, Jafari A, Alipour R, Ghoranneviss M. The effects of growth time on WO<sub>3</sub> nanostructure synthesized by HFCVD method. *J Fusion Energy.* 2015;34(5):1157-61.
- Zhu J, Vasilopoulou M, Davazoglou D, Kennou S, Chroneos A, Schwingenschlogl U. Intrinsic defects and H doping in WO<sub>3</sub>. *Sci Rep.* 2017;7:40882.
- Yousaf A, Imran M, Zaidi S, Kasak P. Highly efficient photocatalytic Z-scheme hydrogen production over oxygen-deficient WO<sub>3</sub>-x nanorods supported Zn<sub>0.3</sub>Cd<sub>0.7</sub>S heterostructure. *Sci Rep.* 2017;7:6574-84.
- Huang R, Shen Y, Zhao L, Yan M. Effect of hydrothermal temperature on structure and photochromic properties of WO<sub>3</sub> powder. *Adv Powder Technol.* 2012;23:211-4.
- Meng D, Wang G, San X, Song Y, Shen Y, Zhang Y, et al. Synthesis of WO<sub>3</sub> flower-like hierarchical architectures and their sensing properties. *J Alloys Compd.* 2015;649:731-8.
- Chang X, Sun S, Yin Y. Green synthesis of tungsten trioxide monohydrate nanosheets as gas sensor. *Mater Chem Phys.* 2011;126(3):717-21.
- Muhammad A, Anurat W, Zoolfakar S, Rosmaliniab K, Wojtek W. Investigation of RF sputtered tungsten trioxide nanorod thin film gas sensors prepared with a glancing angle deposition method toward reductive and oxidative analytes. *Sens Actuators B Chem.* 2013;183:364-71.
- Vallejos S, Khatko V, Calderer J, Gracia I, Cane C, Llobet E, et al. Micro-machined WO<sub>3</sub>-based sensors selective to oxidizing gases. *Sens Actuators B Chem.* 2008;132(1):209-15.
- Long H, Zeng W, Zhang H. The solvothermal synthesis of the cobweb-like WO<sub>3</sub> and its enhanced gas-sensing property. *Mater Lett.* 2017;188:334-7.